Thermal emission and design in one-dimensional periodic metallic photonic crystal slabs

David L. C. Chan, Marin Soljačić, and J. D. Joannopoulos
Department of Physics and Center for Materials Science and Engineering, Massachusetts Institute of Technology, Cambridge, Massachusetts 02139, USA
(Received 4 April 2006; published 26 July 2006)

We present a useful framework within which we can understand some of the physical phenomena that drive thermal emission in one-dimensional periodic metallic photonic crystals, emphasizing phenomenology and physical intuition. We perform detailed numerical calculations for these systems and find that polarization and periodicity play key roles in determining the types of physical phenomena that can arise. Two promising structures are identified as good candidates for thermal design. We conclude with a discussion of how the emissive properties of these systems can be tailored to our needs.

DOI: 10.1103/PhysRevE.74.016609 PACS number(s): 42.70.Qs, 65.40.−b, 78.20.Bh, 78.67.−n

I. INTRODUCTION

The physics of blackbodies has been a source of fascination and scientific research for well over a century now [1]; properties of their thermal emission provided one of the most important clues for the discovery of quantum mechanics. In practice, most objects have only finite absorption, and are thus referred to as "graybodies." By virtue of Kirchhoff's law, these objects also have subunity emissivity. However, graybodies are of interest because their thermal emission spectra can be changed by altering the geometry of the system or the materials used. The ability to modify or tailor the thermal emission profile of an object is of great importance and interest in many areas of applied physics and engineering. It has been noted recently that periodic subwavelength scale patterning of metallodielectric systems, i.e., photonic crystals, can modify their emission spectra in many interesting ways [2–7], through various physical effects such as surface plasmons [8–10], resonant-cavity enhancement [11], Bragg reflection [12], and modification of density of states via photonic band gaps [12–15]. Thus a clear and physically intuitive understanding of the mechanisms that can arise in such systems is of great value in guiding thermal design.

In this work, we focus on some of the most important physical phenomena that give rise to many of the features observed in thermal emission spectra of one-dimensional (1D) periodic metallic photonic crystal slabs, with the intention of developing physical intuition and understanding of features of emission spectra. We study these systems and demonstrate through detailed numerical studies the intricate dependence of these excitations on polarization, and how the type of periodicity can affect the characteristics of thermal emission spectra we observe. This enables us to analyze the emission spectra of 1D periodic metallic photonic crystal slabs in order to identify, with confidence, the underlying physical phenomena and to understand the physics behind them; this way, we show how one can tailor the thermal emission properties of these structures to achieve one's design needs. For definiteness, we focus our attention on emission in the direction perpendicular to the plane of the slab.

This paper is organized as follows: in Sec. II, we discuss the various physical phenomena that can influence the emission spectra of 1D periodic metallic photonic crystal slabs. Section III outlines the numerical methods we use in our calculations. In Sec. IV, we examine the role of polarization in these systems. In Sec. V, we turn our attention to periodicity and how it can give rise to surface plasmon excitations. Section VI discusses the dependence of emission spectra on metallic material parameters, while in Sec. VII, we give consideration to the role of diffraction and its influence on emission spectra. In Sec. VIII, we show how the physical intuition and understanding developed in earlier sections can help us design the thermal emission spectra of these systems.

II. PHYSICAL PHENOMENA THAT INFLUENCE EMISSION SPECTRA

Kirchhoff's law states that for an object in thermal equilibrium with the surrounding radiation field, its absorptivity and emissivity are equal, for every frequency, direction, and polarization. Thus, to study thermal emission of an object, we need simply calculate its absorptivity spectrum, knowing that the object's absorptivity and emissivity spectra are identical. Moreover, for the purposes of developing an intuitive understanding of the physics behind thermal emission, it is often more helpful to think in terms of absorption rather than emission, and it is on this basis that we proceed.

In a 1D periodic metallic photonic crystal (PhC) slab, there is a marked distinction between the two orthogonal directions within the plane of the slab (see graphic insets in Fig. 1). One direction (we shall call this x) is the direction of the PhC's periodicity, and is characterized by the existence of a discrete translational symmetry. The other direction (we shall call this y) supports continuous translational symmetry. The two types of translational symmetry can lead to drastically different physical effects in a 1D periodic metallic PhC slab. Some of the phenomena that can be observed can be broadly described as waveguide cut-offs, waveguide resonances, surface plasmons, and diffraction peaks. Each of these phenomena leaves a characteristic mark on the emission or absorption spectra. In our examination of the significant role played by polarization and periodicity in the physics of these systems, we will come across each of these interesting phenomena in turn. In this section, we give brief descriptions of these phenomena.

First, it is important to note that because of the mirror symmetry of the system in a plane perpendicular to y (i.e., the xz plane), the modes of the system can be separated into transverse electric (TE) and transverse magnetic (TM) modes

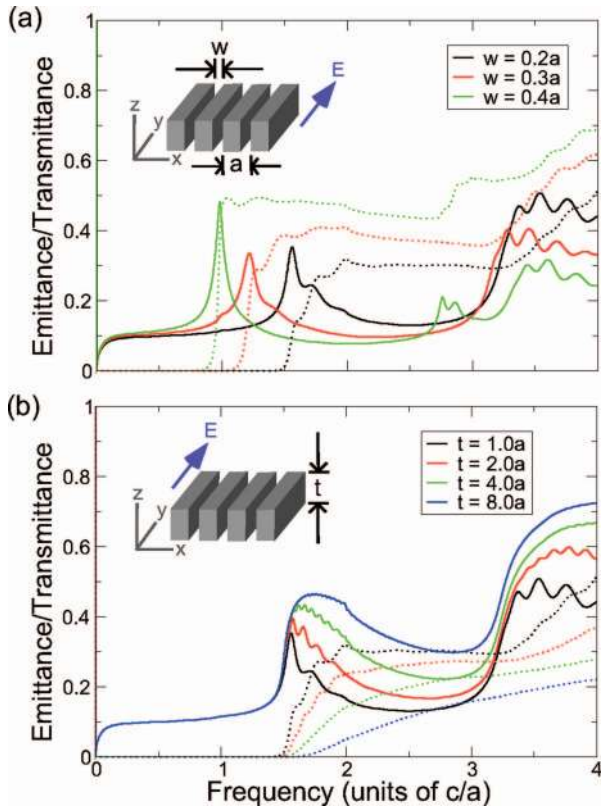

FIG. 1. (Color) Here we show emittance (solid lines) and transmittance (dotted lines) spectra for y-polarized light emitted from a 1D periodic metal slab with gaps, viewed in the perpendicular direction. The Drude parameters used are $\epsilon_\infty=1$, $\omega_0=0$, $\gamma=0.15(2\pi c/a)$, and $\omega_p=\sqrt{10}(2\pi c/a)$. In panel (a), we fix the thickness of the slab at $1.0a$ (where a is the lattice constant of the slab) and vary the width of the gaps. In panel (b), we hold the gap width constant at $0.2a$ and vary the thickness of the slab.

with respect to the mirror plane. In general, given a mirror plane reflection M, separation of modes is only possible at points satisfying $M\mathbf{r}=\mathbf{r}$ and $M\mathbf{k}=\mathbf{k}$ (see Ref. [16]). While there are other mirror planes, such as M_x (for yz planes), these are not origin-independent because of periodicity in the x direction. In our 1D periodic geometry, M_y is the only mirror plane symmetry that is independent of origin, so this is the only way to classify modes into TE and TM for these systems. TE modes have field components E_x, E_z, and H_y, and are even with respect to M_y. TM modes, on the other hand, have field components H_x, H_z, and E_y, and are odd with respect to the same mirror operation. Incident and outgoing light polarized in the x direction can couple to TE modes while y-polarized light can couple to TM modes. Thus we can analyze these two types of modes completely separately, and this is what we do in all our calculations.

Consider again the structure in Fig. 1. If we illuminate the structure with light incident from the top of the cell, the air gaps in the metal slab can be thought of as metallic waveguides channeling light downwards in the direction of $-z$. In other words, the light is propagating between two metal slabs that are infinite in the y direction. Waveguide cut-offs arise from the requirement that the parallel component of the electric field (i.e., E_y in our case) be continuous across a boundary. Inside a perfect metal, the electric field is strictly zero. For such a material, E_y is constrained to vanish at the surface, and this leads to the well-known cutoff frequency corresponding to a half-wavelength oscillation in the x direction. Below this frequency, no propagating mode can be supported within the waveguide, because the boundary condition cannot be satisfied. For a realistic metal (i.e., one that permits some penetration of fields), the fields do not exactly vanish at the surface, but decay away rapidly and exponentially once inside the material. Such boundary condition matching leads to a similar cutoff as in the case of the perfect metal, except that the penetration of field into the metal produces a cutoff with a slightly lower frequency, because the *effective* width of the waveguide in the x direction is slightly larger. Cutoff frequencies depend on the width of the waveguide. The wider the waveguide, the lower the cutoff frequency. No such boundary condition holds for light polarized in the x direction, so there is no waveguide cutoff for that polarization.

Continuing with the same waveguide setup, there exists another phenomenon which applies equally to light of either polarization. Waveguide resonances are analogous to Fabry-Perot resonances except that they take place within a waveguide "cavity." Any narrow channel through which light is forced to propagate can be thought of as a Fabry-Perot cavity with partially reflecting mirrors at either end. If the incoming radiation is of a frequency such that the length of the cavity is equal to an integer number of half wavelengths, we observe resonant transmission of light. We can think of these waveguide resonances as the consequence of boundary impedance matching in the longitudinal (z) direction. These resonances give rise to sharp peaks in the absorbance or emittance spectrum. Although this physical effect can be seen for either polarization of incident light, it is most prominent for light polarized in the x direction whose spectra are not dominated by the existence of waveguide cutoffs.

Surface plasmons (SPs) are excitations that exist on the interface between a plane metal and a dielectric. They are confined to the surface, but can propagate freely within that surface. They have a relatively simple dispersion relation that is approximately linear at low wave vectors and bends over toward a flat cutoff at higher wave vectors ($\omega_p/\sqrt{\epsilon+1}$ is the cutoff frequency, where ω_p is the plasmon frequency and ϵ is the dielectric constant). If the direction of propagation is x (i.e., $\mathbf{k}$ is in the x direction), then the SP will have field components E_x, E_z, and H_y (the z direction is normal to the interface). The SPs are unusual in that they have an electric field component in the direction of propagation. Light incident from air cannot couple into SP modes since all SP modes are below the light line of air. However, it *can* couple into SP modes if the wave vector of the SP is along a direction of discrete translational symmetry, because in such a direction, wave vector is conserved only up to an integer multiple of the reciprocal lattice vector. These correspond to $k=1,2,3\ldots$ in units of $2\pi/a$. Thus for our structure in Fig. 1, normally incident light polarized in x can couple into SPs propagating in the x direction. In contrast, normally incident light polarized in y cannot couple into any SP modes.

Diffraction peaks occur when we consider the slab system at a macroscopic level, in terms of incoming and outgoing

radiation modes. This effect is not unique to metallic PhCs, and can be observed in nonmetallic PhCs as well. In terms of absorption, the incident light can couple to outgoing radiation modes (in transmission or reflection) that conserve the wave vector in the x direction (k_x) up to a reciprocal lattice vector, since that is the direction of discrete periodicity. Because the incident light has no k_x component, it can couple to outgoing modes with k_x equal to an integer multiple of $2\pi/a$ (i.e., 1 in our units). This means that as we increase the frequency of the incoming radiation, a new diffraction direction will be coupled into at $\omega=1,2,3\ldots$ (in units of $2\pi c/a$), corresponding to $k_x=1,2,3\ldots$ (this correspondence holds because the light is incident from vacuum, which has a linear dispersion relation). At the threshold frequency for a new diffraction mode, the wave vector has no real k_z component, and so **k** is parallel to the surface of the slab. Such "grazing" modes have maximum interaction with the slab because they travel close to the surface of the metal, and as such are strongly absorbed by the material. These absorption peaks translate into emission peaks, via Kirchhoff's law, so we would expect to see emission peaks for modes corresponding to $\omega=k=1,2,3\ldots$.

III. DESCRIPTION OF NUMERICAL METHODS

Before presenting our results, a brief description of our methods is in order. Numerical simulations in our work are performed using a finite-difference time-domain (FDTD) algorithm [17]. These are exact (apart from discretization) solutions of 3D Maxwell's equations, including material dispersion and absorption. We choose a computational cell with dimensions $40\times2\times240$ grid points, corresponding to 40 grid points per lattice constant a. This is essentially a 2D simulation, because k_y is constrained to be zero by periodic boundary conditions on opposite y faces of the computational cell. The PhC slab is in the middle, and flux planes are placed on either side of it at least $2a$ away. We run the simulation for a total of 40 000 time steps, chosen to be sufficiently large to allow resolution of peaks with quality factors (Q) up to 250. We illuminate the photonic crystal slab with a normally incident, temporally Gaussian pulse. We record the fields going through flux planes on either side of the slab and perform a discrete Fourier-transform on the time series of fields, which we use to calculate fluxes as functions of frequency [$\Phi(\omega)$]. We run the simulation once with the slab in place, and again with vacuum only. The reflectance is given by $R(\omega)=[\Phi_1^{vac}(\omega)-\Phi_1^{slab}(\omega)]/\Phi_1^{vac}(\omega)$ where the flux plane closer to the light source is "1," and the flux plane further from the light source is "2." Note that in vacuum, $\Phi_1^{vac}(\omega)=\Phi_2^{vac}(\omega)$. The transmittance is given by $T(\omega)=\Phi_2^{slab}(\omega)/\Phi_2^{vac}(\omega)$ and the absorbance is simply $A(\omega)=1-R(\omega)-T(\omega)$. This way, we obtain reflectance, transmittance and absorbance spectra for PhC slabs. We incorporate absorption into our simulations by means of the Drude model, according to the following equation:

$$\epsilon(\omega)=\epsilon_\infty+\omega_p^2/(\omega_0^2-\omega^2-i\gamma\omega),$$

where ϵ_∞, γ, ω_0, and ω_p are input parameters. In our case, we are concerned with metals, for which $\omega_0=0$. (For metals, ω_p is known as the plasmon frequency.) By Kirchhoff's law, the absorbance spectra so calculated are identical to the emittance spectra of these objects, for each polarization, frequency, and observation angle.

TABLE I. The waveguide cutoff frequencies associated with different gap widths in Fig. 1(a), and their corresponding half wavelengths.

w	Cutoff	$\lambda/2$
0.2	0.984	0.32
0.3	1.22	0.41
0.4	1.56	0.51

IV. ROLE OF POLARIZATION

Let us now make our discussion more concrete by considering a real 1D system. We study a 1D periodic metal slab with gaps (as in Fig. 1) by calculating the emittance of such an object in the perpendicular direction. For now, we focus on y-polarized light, i.e., light polarized in the direction of *continuous* translational symmetry. Figure 1(a) shows the emittance spectrum for this structure for a few different gap widths. [We include the transmittance spectrum (dotted lines) for completeness.] The first peak we see in emittance, whose frequency varies with the gap width, corresponds to the waveguide cutoff that we described earlier, which is the frequency at which one can just fit approximately half a wavelength into the gap in the x direction. In reality, there is penetration of evanescent waves into the surrounding metal in the x direction which makes the gap effectively wider than it is. As we increase the gap width, the waveguide cutoff frequency decreases, as expected. From the frequencies of the peaks, we can deduce the half wavelength associated with these cutoffs, and we find that they are slightly larger than the widths of the gaps, as predicted (see Table I). The half wavelengths are about $0.1a$ larger than the actual gap widths, demonstrating penetration of fields into the bulk of the metal. In Fig. 1(b), we hold the gap width constant and vary the thickness of the slab. The waveguide cutoff is clearly seen around $\omega\approx1.5c/a$, and is the same for all thicknesses. The dotted lines show transmittance decreasing with increasing slab thickness; as expected, more light is being absorbed while propagating through longer waveguides. Notice the small oscillations between $1.5c/a$ and $2.0c/a$. These are the waveguide resonances we discussed earlier. The number of such oscillations increases with the thickness of the slab. Indeed, we see that the red curve has twice as many oscillations as the black curve, and the green curve twice as many as the red curve, and so on. We took the four peaks from the red curve, recorded their frequencies, and calculated their half wavelengths in the z direction (see Table II). The half wavelengths ($\lambda_z/2$) are calculated using the formula $(\omega/c)^2=(2\pi/\lambda_x)^2+(2\pi/\lambda_z)^2$, where λ_x is the half wavelength in the x direction (obtained from Table I) and λ_z is the half wavelength in the direction of guided propagation. In the third column of Table II, we put the expected and pre-

TABLE II. The waveguide resonant frequencies associated with the red curve in Fig. 1(b), and their corresponding half wavelengths, calculated and predicted.

Freq.	$\lambda/2$	$2/n$
1.577	2.20	2
1.658	0.89	1
1.760	0.61	$2/3$
1.880	0.48	$1/2$

dicted number of half wavelengths that fit into the vertical cavity. For example, the nth-order harmonic fits n half wavelengths into the waveguide in the z direction, so we would expect to see a half wavelength of $2/n$ in units of a, since the thickness of the slab is $2.0a$. Assuming the first peak listed in Table II is the second harmonic, we see good correspondence between the half wavelengths calculated from the emission peaks and the expected half wavelengths. Thus we can be confident that the peaks in the frequency range 1.5–2.0 are due to Fabry-Perot resonances in the waveguides.

In both panels of Fig. 1, we see a dramatic rise in transmittance and emittance above $\omega_p=\sqrt{10}\approx 3.16$ because the material behaves as a regular dielectric (rather than metal) above the plasmon frequency. We see some oscillations above $3.25c/a$; these are dielectric slab resonances, which are analogous to waveguide Fabry-Perot resonances except that they permeate the entire slab. Once again, the number of oscillations increases with increasing slab thickness. Thus we see relatively simple physical effects for incident light polarized in the y direction.

Significantly different emission and transmission characteristics can be observed for the same structure for light of an orthogonal polarization (i.e., polarized in the x direction). Since Maxwell's equations do not require that the perpendicular component of electric field (E_x) be continuous across a boundary, the waveguide cutoffs in the x direction no longer exist. Instead, we expect to see resonances in the z direction within the waveguide cavity. We study the same 1D periodic metal slab with gaps as in Fig. 1, except that this time, we focus on emitted light polarized in the x direction, the direction of *discrete* translational symmetry. In Fig. 2(a), we show emittance and transmittance spectra for this system as a function of gap width. First, we notice that there is high transmittance (dotted lines) at nearly all frequencies shown. Contrast this with Fig. 1(a), which had zero transmittance for frequencies below the waveguide cutoff at $\omega\approx 1$. The two lowest frequency emittance peaks in the black curve are waveguide cavity resonances [we shall discuss this further in Fig. 2(b)]. Between $\omega=1$ and $\omega=\omega_p\approx 3.16$, the spectra shown here are very different from those in the corresponding frequency range in Fig. 1(a). However, above the plasmon frequency, the entire structure behaves as a dielectric, and the differences between the two polarizations are no longer as pronounced. Indeed, we observe similar emittance curves for both polarizations above the plasmon frequency (high transmittance and slab resonances which increase in number with thickness).

In Fig. 2(b), we hold the gap width constant at $0.2a$ and vary the thickness of the slab. The most interesting phenomenon here is the number of sharp peaks between $\omega=0$ and $\omega=1$. The fact that their number and density increase with the thickness of the slab is clear evidence that they are produced by waveguide resonances in the z direction. To confirm this suspicion, we plot the field profiles for two resonances on the red curve (first and fourth resonances), as indicated by the two black arrows (I and II). For each resonance, we plot E_x and E_z side by side. The resonances were excited by normally incident light coming down from the top of the computational cell, in the absorbance setup. We notice that the first resonance has one E_x node within the waveguide in the z direction. For the fourth resonance on the red curve, we expect four nodes, and indeed this is what we find. Although in (I) we see that E_x has one node in the middle of the waveguide, it is in fact the lowest order mode because H_y (not shown), which is related to $\partial E_x/\partial z$ through Ampère's law, has a maximum at that same point in the middle of the waveguide, and no node. (Note that H_y is a scalar in this case because we are considering a TE mode which has only one component of magnetic field in the y direction.) Another interesting feature is the nodal line in E_z down the middle of the waveguide. This arises because E_z is given by $\partial H_y/\partial x$ (from Faraday's law). Since there is a maximum in H_y as we traverse the waveguide in the x direction, there is a node in E_y. Note also that the node in E_x is shifted upwards from the center of the waveguide because the incident wave coming down from the top of the cell interacts with the resonance inside the waveguide in such a way as to shift the position of the node of the combined fields upwards.

In Fig. 2(c), we study a corrugated metal slab, for various gutter widths, in order to see how things are different when we prevent direct transmission of light through the solid. First of all, above the plasmon frequency we see the same transparent behavior and the familiar dielectric slab resonances. However, the rest of the emittance spectrum looks very different. To better understand some of these modes, we show field profiles for three of the peaks on the green curve (III–V). In each set of field plots, we can see the incident beam and also a sort of cavity mode inside the gutter. These cavity modes are analogous to the case when we had gaps or waveguides in the metal, except that they are terminated differently: instead of being terminated with air, they are terminated with metal. This is most pronounced in the case of (V) ($\omega\approx 1.8$), which shows strong fields being pinned to the corners and edges of the gutter.

Thus we see that polarization plays a key role in 1D periodic systems. Because one kind of polarization sees a continuity boundary condition when impinging on a metallic surface and the other does not, drastically different physical effects are observed. In the next section, we discuss the intricate connection between periodicity and surface plasmons.

V. PERIODICITY AND SURFACE PLASMONS

Most of the physical effects we have seen so far have been explainable in terms of Maxwell boundary conditions which require us to fit an integer or half integer number of wavelengths within a particular resonant cavity. We now turn our attention to a totally different type of physical phenom-

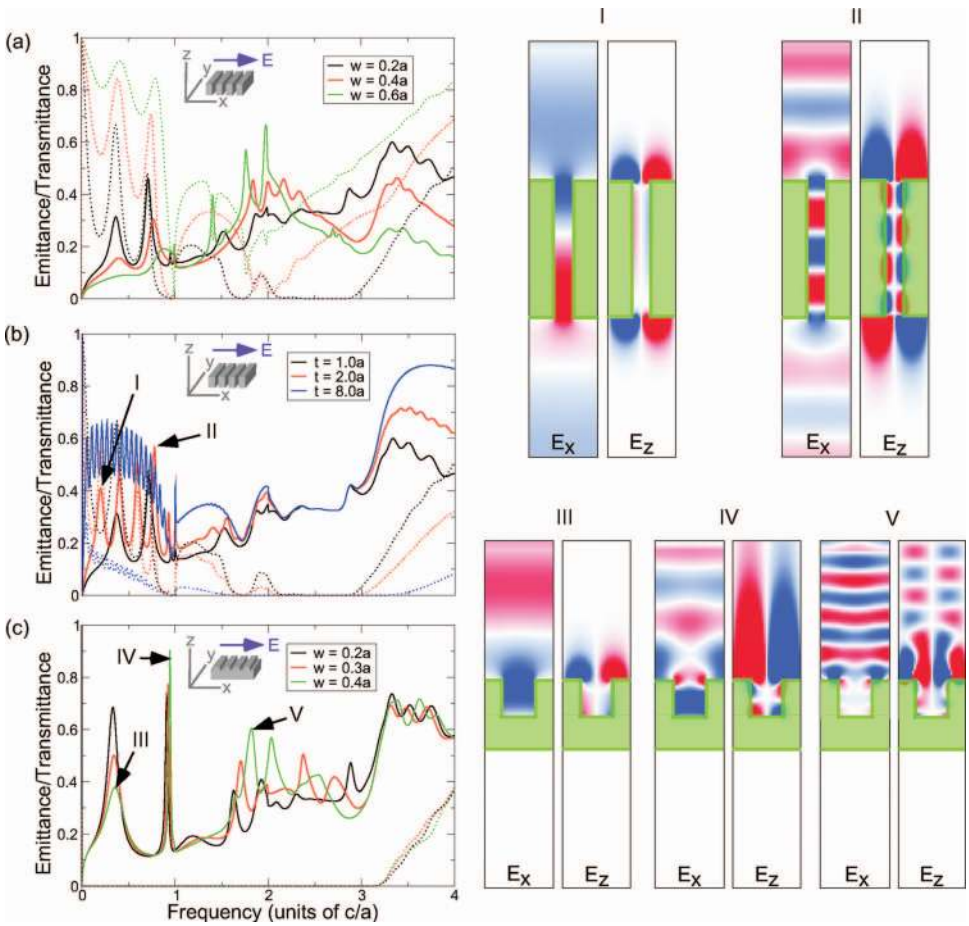

FIG. 2. (Color) We show emittance (solid lines) and transmittance (dotted lines) spectra for a 1D periodic metal slab in the perpendicular direction and light polarized in the x direction. The Drude parameters used are $\epsilon_\infty=1$, $\omega_0=0$, $\gamma=0.15(2\pi c/a)$, and $\omega_p=\sqrt{10}(2\pi c/a)$. In panel (a), we fix the thickness of the slab at $1.0a$ and vary the width of the gaps. In panel (b), we hold the gap width constant at $0.2a$ and vary the thickness of the slab. In panel (c), we study a corrugated metal slab of thickness $1.0a$ with a gutter of depth $0.5a$, for different gutter widths. To better understand some of the modes exhibited in these panels, we show field profiles for peaks labeled I–V on the right half of the figure. Each pair of field plots shows E_x on the left and E_z on the right. The edges of the computational cell are marked by thin black lines, while the metallic structure is shown in a translucent green color with dark green borders. The incident beam comes down from the top of the cell.

enon, one which does not arise from such resonances in cavities: surface plasmons. These are affected by periodicity because wave vector has to be conserved up to a reciprocal lattice vector in a direction of periodicity; however, along a direction of continuous translational symmetry, wave vector has to be absolutely conserved. Since the x direction is, in our case, discretely periodic, normally incident light polarized in x can couple into SP modes with integer k (in units of $2\pi/a$). The y direction, however, has continuous translational symmetry, so incident light polarized in y cannot couple into SP modes in the system.

We consider a uniform metal slab with small dielectric strips on its surface. We excite SP modes in the system, and they emit light in the perpendicular direction, polarized in the x direction. Figure 3(a) shows how emittance and transmittance vary with the dielectric constant of the strip (ϵ). First, we observe many peaks in the emittance spectra, and we note that the frequencies of these peaks decrease with increasing ϵ. Second, we see zero transmittance in the system for frequencies below $\omega_p \approx 3.16$, as we expect, because the metal is opaque at frequencies below the plasmon frequency. Third, we demonstrate that most of the emittance peaks with frequencies below 2.0 observed in Fig. 3(a) are in fact produced by SPs.

To show this, we record the frequencies of the peaks (up to $\omega_p/\sqrt{\epsilon+1}$, the SP cutoff) for each curve in panel (a), and plot them as circles (red circles corresponding to red peaks, for example), making the assumption that the first peak has a wave vector of $1.0(2\pi/a)$, the second has a wave vector of $2.0(2\pi/a)$, and so on. We make this assumption because, as we have said, normally incident light can only couple to SP modes with integer wave vectors (in units of $2\pi/a$) in the direction of periodicity. Thus we expect to see successive SP peaks with increasing frequencies corresponding to $k=1,2,3\ldots$ SP modes. In addition, we plot SP dispersion curves for uniform and semi-infinite metal-air and metal-dielectric structures (dotted lines). Surface plasmon modes in the periodic structure under consideration would therefore be expected to have a dispersion relation that lies between different SP dispersion relations of the case when the dielectric is uniform. For example, we would expect the red circles to lie between the black and red dotted curves, the green circles

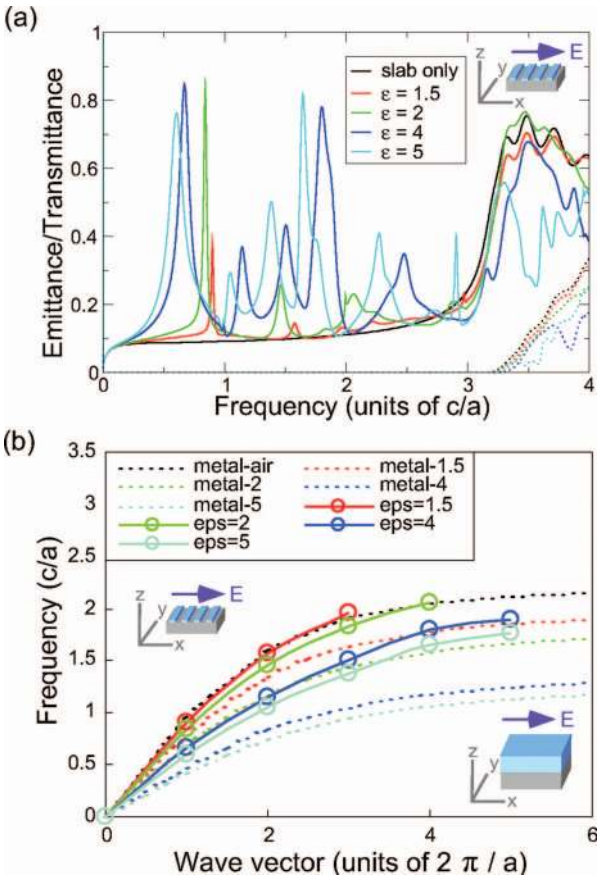

FIG. 3. (Color) We present emittance (solid lines) and transmittance (dotted lines) spectra for a uniform metal slab with thin dielectric strips periodically distributed on its surface. We consider light emitted or transmitted in the perpendicular direction and polarized in the x direction. The dielectric structure has a rectangular cross section of width $0.5a$ and height $0.2a$, and sits on top of a metal slab of thickness $1.0a$. The metal has Drude parameters $\epsilon_\infty = 1$, $\gamma = 0.15(2\pi c/a)$, and $\omega_p = \sqrt{10}(2\pi c/a)$. Panel (a) shows how emittance and transmittance vary for a few different dielectric constants of the strips. In panel (b), we plot the frequencies of some of the peaks in panel (a) as circles (red circles corresponding to red peaks, for example). In addition, we plot SP dispersion curves for uniform, semi-infinite metal-air and metal-dielectric structures (dotted lines). Top-left inset shows structure described by solid lines; bottom-right inset shows structure described by dotted lines.

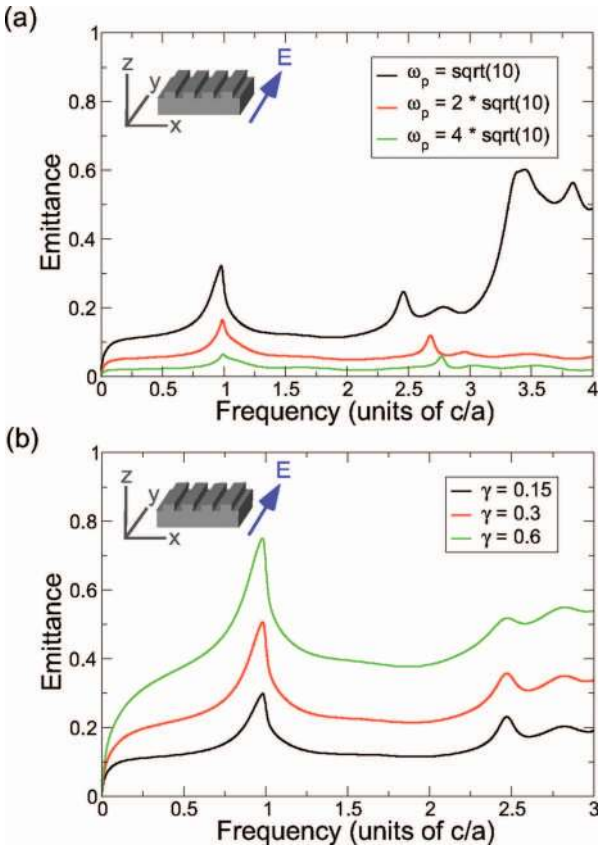

FIG. 4. (Color) Emittance spectra for a corrugated metal slab, for y polarization in the perpendicular direction. The metal slab has thickness $1.0a$, with gutters of depth $0.5a$ and width $0.5a$. The metal has the usual Drude parameters of $\epsilon_\infty = 1$, $\gamma = 0.15(2\pi c/a)$, and $\omega_p = \sqrt{10}(2\pi c/a)$. In panel (a), we show how emittance changes with the plasmon frequency (ω_p). Panel (b) shows the variation of emittance with γ, the parameter that controls material losses in the Drude model (in this case $\omega_p = \sqrt{10}$). Note that in both panels, clear diffraction peaks are seen at $\omega = 1$, and the positions of these peaks do not change with either ω_p or γ.

to lie between the black and green dotted curves, and so on. Indeed, this is exactly what we see. Furthermore, the fact that the circles, when joined together by solid lines, form a dispersion relation that clearly bends over toward a cutoff, gives us confidence in identifying these modes as surface plasmons. Note also that, in Fig. 3(a), no SP peaks are observed in the case of the uniform and unperturbed metal slab (black curve), just as expected: in that case, continuous translational symmetry in the x direction is maintained, so incident light cannot couple to the SP modes of the system.

VI. DEPENDENCE ON METALLIC MATERIAL PARAMETERS

We have seen the pivotal role played by polarization in the kinds of modes we can thermally excite in a 1D periodic metallic PhC slab system. We have also examined the conditions under which SP modes can be excited, and the relation of these modes to the type of translational symmetry exhibited by the structure (continuous or discrete). With this knowledge, we can design, analyze, and understand a diverse array of 1D periodic metallic PhC slab structures. For completeness, we examine a few other interesting physical effects which can arise in such systems.

This time, we study light emanating from a corrugated metal slab in the perpendicular direction and polarized in the y direction. In Fig. 4(a), we show how emittance changes with the plasmon frequency (ω_p) of the metal. One can easily observe an inverse proportionality relationship between background emittance and ω_p. Using the Drude model, we can show that in the regime specified by $\gamma \ll \omega \ll \omega_p$, the absorbance, and therefore the emittance, is given approximately by $2\gamma/\omega_p$.

Consider light incident on a semi-infinite slab of metal with dielectric function

$$\epsilon(\omega) = 1 - \frac{\omega_p^2}{\omega^2 + i\gamma\omega},$$

where we have chosen $\epsilon_\infty = 1$ and $\omega_0 = 0$, as is consistent with our numerical calculations. Breaking this up into real and imaginary parts, we have

$$\epsilon_1 = 1 - \frac{\omega_p^2/\gamma^2}{1 + \omega^2/\gamma^2}, \tag{1}$$

$$\epsilon_2 = \frac{\omega_p^2/\gamma}{\omega(1 + \omega^2/\gamma^2)}. \tag{2}$$

We can convert these into expressions for the real and imaginary parts of the refractive index, using the equality $\epsilon_1 + i\epsilon_2 = (n+ik)^2$. Making the approximation $\gamma \ll \omega \ll \omega_p$, we have

$$n = \frac{\gamma\omega_p}{2\omega^2}, \tag{3}$$

$$k = \omega_p/\omega. \tag{4}$$

For a semi-infinite slab of metal, the reflectance (R) is given by

$$R = \frac{(n-1)^2 + k^2}{(n+1)^2 + k^2}.$$

Substituting our expressions for n and k into the above expression yields, approximately,

$$R \approx 1 - \frac{2}{\omega_p/\gamma}$$

from which the absorbance (A) follows:

$$A \equiv 1 - R = \frac{2\gamma}{\omega_p}. \tag{5}$$

Although we have done this calculation for a semi-infinite slab, it is a good approximation for any finite slab whose thickness is much greater than the skin depth of the metal. For $\omega_p = \sqrt{10}(2\pi c/a)$ and $\gamma = 0.15(2\pi c/a)$, one can show that the skin depth is $\sim 0.25a$ for $\omega = 2(2\pi c/a)$. This confirms that we are working in the regime where the skin depth is much smaller than the thickness of the slab (in this case, $1.0a$). We therefore observe, in Fig. 4, precisely the above inverse proportionality relationship between absorbance and ω_p.

Again, we see, for the black curve, that emittance increases significantly at frequencies above $\omega_p = \sqrt{10} \approx 3.16$, because above the plasmon frequency the metal becomes transparent to incident radiation, which penetrates the whole structure, leading to greater absorption and thereby greater emission. (This is not seen in the red and green curves because their plasmon frequencies are out of the plotting range.) Figure 4(b) shows the variation of emittance with γ, the parameter that controls material losses in the Drude model. We observe that the background emittance increases almost linearly with increasing γ. This can be understood by considering $\mathrm{Im}(\epsilon) \sim \gamma/\omega(\omega^2 + \gamma^2)$, which, for high frequencies ($\omega \gg \gamma$), is roughly linear in γ. This is also consistent with Eq. (5), which is approximate. Finally, we point out that in both panels, clear diffraction peaks are seen at $\omega = 1$, and the positions of these peaks do not change with either ω_p or γ.

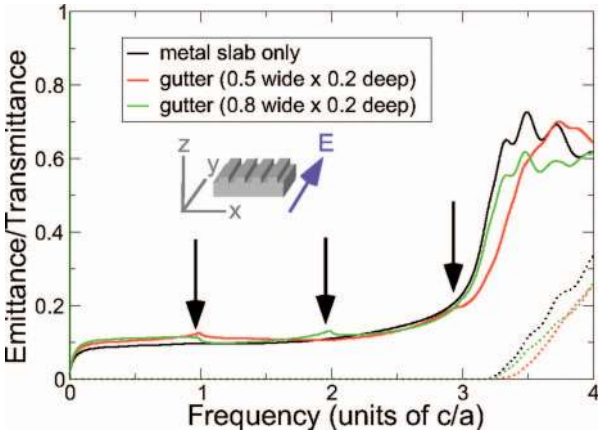

FIG. 5. (Color) We show emittance and transmittance spectra for a corrugated metal slab produced by normally incident light, polarized in the y direction, for two different gutter widths. The metal has Drude parameters $\epsilon_\infty = 1$, $\gamma = 0.15(2\pi c/a)$, and $\omega_p = \sqrt{10}(2\pi c/a)$. The metal slab has thickness $1.2a$, with gutters of depth $0.2a$ and width $0.5a$ (red curve) and $0.8a$ (green curve). We observe that there are small emittance peaks at integer frequencies ($\omega = 1, 2, 3$, indicated by black arrows), caused by diffraction. Notice that no diffraction peaks are seen in the case of a uniform metal slab (black curve), because such a slab has continuous translational symmetry in the x direction. Note also the sudden rise in transmittance and emittance above the plasmon frequency ($\omega_p \approx 3.16$), above which the metal is transparent.

VII. ROLE OF DIFFRACTION

In Fig. 5, we show emittance and transmittance spectra for a corrugated metal slab for normally incident light polarized in the y direction, for two different gutter widths. We observe that there are small emittance peaks at the integer frequencies ($\omega = 1, 2, 3$). These peaks are caused by diffraction. The size of these diffraction peaks depends on the geometry of the system and the materials used. Notice that diffraction peaks do not appear in the case of a uniform metal slab (black curve), because such a slab has continuous translational symmetry in the x direction. This symmetry implies that the transverse wave vector is *absolutely* conserved, with the consequence that only modes for which $k_x = 0$ can couple to outgoing modes in the perpendicular direction. In other words, a uniform metal slab is unable to produce diffracted beams. Note also the sudden rise in transmittance and emittance above the plasmon frequency ($\omega_p \approx 3.16$), above which the metal acts as a dielectric.

VIII. THERMAL DESIGN

Now that we have a good understanding of the physical effects that thermal emission can produce, we turn our attention to thermal design using 1D periodic metallic PhCs. Of

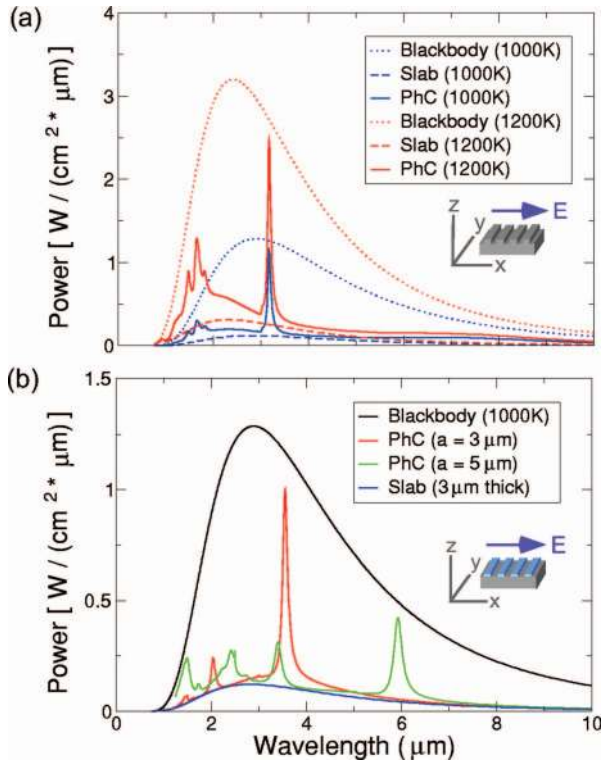

FIG. 6. (Color) Panel (a) shows how emissive power for a corrugated metal slab changes with temperature of operation. The emission spectra is observed in the perpendicular direction, polarized in the x direction. The metal has Drude parameters $\epsilon_\infty=1$, $\gamma/(2\pi c)=500\ \mathrm{cm}^{-1}$, and $\omega_p/(2\pi c)=10\,540\ \mathrm{cm}^{-1}$. The metal slab has thickness 3 μm, with gutters of depth 1.5 μm and width 1.2 μm. We show the spectra for the blackbody, the PhC, and the uniform metal slab (thickness 3 μm) for two temperatures, 1000 and 1200 K. Panel (b) shows how emissive power for a metal slab with dielectric strips changes with the lattice constant. The metal slab is of thickness 3 μm, while the dielectric strips are of width 1.5 μm, height 0.6 μm, and $\epsilon=2$. Clearly, increasing the lattice constant increases the wavelength at which peak emission occurs. Note that the peaks arise from the excitation of surface plasmon modes.

the many systems we studied in this work, the corrugated metal slab and the slab with dielectric strips are the most promising in terms of emissivity enhancement, and it is to these two structures that we devote our attention. Figure 6(a) shows the power emitted by a corrugated metal slab [identical to the one in Fig. 2(c)], at two different temperatures (1000 and 1200 K). We show also emission spectra for a blackbody (the Planck distribution) and a uniform slab for comparison. First, we notice that the positions of the peaks do not change with temperature. Second, increasing temperature increases emission at *all* wavelengths, as expected by Stefan's law. Third, the relative weighting given to different wavelengths changes with temperature, because the peak of the Planck distribution shifts toward lower wavelengths with increasing temperature. In our case, the group of small peaks between 1 and 2 μm were insignificant features at 1000 K, but became much more prominent at 1200 K, because the blackbody spectrum shifted in such a way as to give those peaks much more weight than before. Fourth, the emission of the photonic crystal slab exceeds that of the uniform slab at all wavelengths and at all temperatures. In fact, the enhancement is impressive: we see a ten-fold increase in emissive power (over that of a slab) at the major peak at around 3.1 μm. Of course, emissivity never exceeds unity, because that would violate the second law of thermodynamics (the large peak in question attains 90% emissivity). The important lesson we learn from this is that we can emphasize different parts of the emission spectrum of a PhC by changing the temperature at which we operate the thermal structure.

In Fig. 6(b), we present the emissive power of a metal slab with dielectric strips on top [similar to the one in Fig. 3(a)]. Here, instead of changing the temperature, we keep temperature fixed and vary the lattice constant of the PhC. The blackbody envelope and the emission spectrum of a uniform slab of this same metal are shown for comparison. We see that increasing the lattice constant shifts the emission peaks in the PhC toward a higher wavelength. In our case, for $a=3$ μm, the large peak is already close to the point of maximum blackbody emission, so that increasing the lattice constant only served to decrease the total emission from that excitation (incidentally, it is a surface plasmon excitation). However, the change in a also brought some small peaks from the lower wavelengths into the picture. Clearly, one has a substantial degree of control over the positions of the peaks. One should realize that in both cases, the emissivity of the peak is unchanged, because PhC emissivity spectra are scale invariant (contrast this with that of a uniform slab, whose absolute emission spectrum does not scale with a, since it has continuous translational symmetry). For both choices of a, there is significant enhancement of emission over that of a uniform slab.

IX. CONCLUSION

We demonstrated a physical and intuitive framework within which the thermal behavior of 1D periodic metallic photonic crystal slabs can be understood. In such systems, polarization and periodicity play key roles in our understanding of waveguide cutoffs, waveguide Fabry-Perot resonances, SP modes, and diffraction peaks. We found that metal slabs with corrugation or dielectric strips are good building blocks for thermal design, because they have strong emission peaks with high emissivity. These peaks can be shifted to the desired wavelength by changing the lattice constant of the system, while other parts of the emission spectrum can be amplified and made more prominent by altering the temperature of operation, which changes the weight given to a particular range of wavelengths. One can use the principles described here to tailor and design thermal emission using 1D periodic metallic photonic crystal slabs.

ACKNOWLEDGMENTS

We thank our colleagues Peter Bermel, Michael Levin, and Bas Overbosch at the Massachusetts Institute of Technology for helpful discussions. This work was supported in part by the Croucher Foundation of Hong Kong and the MRSEC program of the NSF under Grant No. DMR-0213282.

[1] M. Planck, Ann. Phys. **4**, 553 (1901).
[2] B. A. Munk, *Frequency Selective Surfaces Theory and Design* (Wiley, New York, 2000).
[3] J.-J. Greffet *et al.*, Nature (London) **416**, 61 (2002).
[4] A. Narayanaswamy and G. Chen, Phys. Rev. B **70**, 125101 (2004).
[5] C. Luo, A. Narayanaswamy, G. Chen, and J. D. Joannopoulos, Phys. Rev. Lett. **93**, 213905 (2004).
[6] S. Enoch *et al.*, Appl. Phys. Lett. **86**, 261101 (2005).
[7] M. Florescu, H. Lee, A. J. Stimpson, and J. Dowling, Phys. Rev. A **72**, 033821 (2005).
[8] T. W. Ebbesen, H. J. Lezec, H. F. Ghaemi, T. Thio, and P. A. Wolff, Nature (London) **391**, 667 (1998).
[9] M. U. Pralle *et al.*, Appl. Phys. Lett. **81**, 4685 (2002).
[10] B. J. Lee, C. J. Fu, and Z. M. Zhang, Appl. Phys. Lett. **87**, 071904 (2005).
[11] I. Celanovic, D. Perreault, and J. Kassakian, Phys. Rev. B **72**, 075127 (2005).
[12] C. M. Cornelius and J. P. Dowling, Phys. Rev. A **59**, 4736 (1999).
[13] S.-Y. Lin *et al.*, Phys. Rev. B **62**, R2243 (2000).
[14] S. Y. Lin, J. Moreno, and J. G. Fleming, Appl. Phys. Lett. **83**, 380 (2003).
[15] S.-Y. Lin, J. Moreno, and J. G. Fleming, Appl. Phys. Lett. **84**, 1999 (2004).
[16] J. D. Joannopoulos, R. D. Meade, and J. N. Winn, *Photonic Crystals: Molding the Flow of Light* (Princeton University Press, Princeton, NJ, 1995).
[17] A. Taflove and S. C. Hagness, *Computational Electrodynamics: The Finite-Difference Time-Domain Method* (Artech House, Norwood, MA, 2000).